Polymeric Nanoparticles to Control the Differentiation of Neural Stem Cells in the Subventricular Zone of the Brain

Tiago Santos,[†] Raquel Ferreira,[†] João Maia,[‡] Fabienne Agasse,[†] Sara Xapelli,[†] Luísa Cortes,[†] José Bragança,[§] João O. Malva,[†] Lino Ferreira,[†,∥,*] and Liliana Bernardino[†,⊥,*]

[†]CNC - Center for Neuroscience and Cell Biology, University of Coimbra, 3004-517 Coimbra, Portugal, [‡]Matera, Biocant Park, Nucleo 4-Lote 4A, 3060-197 Cantanhede, Portugal, [§]Institute for Biotechnology and Bioengineering, Centre for Molecular and Structural Biomedicine (CBME), University of Algarve, 8005-139 Faro, Portugal, [∥]Biocant - Center of Innovation in Biotechnology, 3060-197 Cantanhede, Portugal, and [⊥]Health Sciences Research Center, University of Beira Interior, 6200-506 Covilhã, Portugal

ABSTRACT Herein, we report the use of retinoic acid-loaded polymeric nanoparticles as a potent tool to induce the neuronal differentiation of subventricular zone neural stem cells. The intracellular delivery of retinoic acid by the nanoparticles activated nuclear retinoic acid receptors, decreased stemness, and increased proneurogenic gene expression. Importantly, this work reports for the first time a nanoparticle formulation able to modulate *in vivo* the subventricular zone neurogenic niche. The work further compares the dynamics of initial stages of differentiation between SVZ cells treated with retinoic acid-loaded polymeric nanoparticles and solubilized retinoic acid. The nanoparticle formulation developed here may ultimately offer new perspectives to treat neurodegenerative diseases.

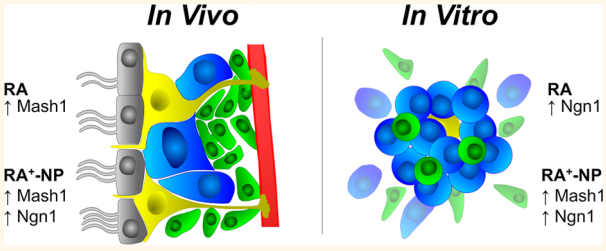

KEYWORDS: retinoic acid · nanoparticles · neural stem cells · neuronal differentiation · subventricular zone

The subventricular zone (SVZ) represents the main germinal neurogenic niche in the adult mammalian brain. Within this region there are self-renewing and multipotent neural stem cells (NSCs) which can ultimately give rise to new neurons, astrocytes, and oligodendrocytes.[1,2] Therefore, driving SVZ stem/progenitor cell differentiation toward the desired cell phenotype may be a promising platform to influence brain regenerative capacities in the setting of diseases, including Parkinson, Alzheimer, and Huntington diseases.[3]

A potential approach to driving the *in vivo* differentiation of SVZ cells involves the efficient delivery of proneurogenic biomolecules into the brain.[4,5] Yet the lack of sustained bioavailability is a major issue in these platforms. Recent studies overcame this obstacle by the delivery of nanoparticles, which were able to provide a sustainable therapeutic effect.[5,6] Unfortunately, the efficacy of these approaches is limited likely due to the poor effect in inducing and controlling the differentiation of SVZ cells. Therefore, the development of new nanoparticle formulations able to release proneurogenic factors in the SVZ cell niche is an utmost need.

Peripheral or central nervous system injury is accompanied by an increased activity of retinaldehyde dehydrogenase. This enzyme is responsible for the conversion of retinaldehyde to retinoic acid (RA).[7] In this context, RA represents a molecule of great importance to modulate neurogenesis, specially the *all-trans* RA isoform. The retinoid signal is transduced in the cell nucleus by heterodimers formed between the retinoic acid receptors (RARs), and the retinoid X receptors (RXRs), which are members of the nuclear receptor superfamily.[8,9] These receptors heterodimerize and bind to a DNA sequence called retinoic acid-response element (RARE), thereby activating gene transcription upon agonist-binding.[10] RA has proven to be capable of inducing neurite outgrowth and neuronal differentiation from various cell sources, including embryonic stem cells (ESCs),[11−13] NSCs,[14,15] dorsal root ganglia,[16]

* Address correspondence to libernardino@gmail.com, lino@biocant.pt.

Received for review January 12, 2012 and accepted November 23, 2012.

Published online November 23, 2012
10.1021/nn304541h

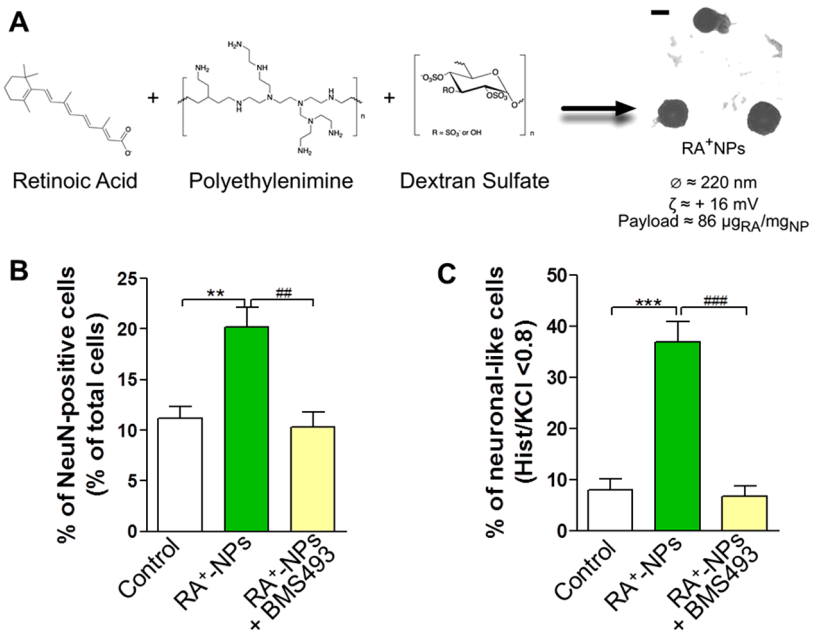

Figure 1. RA$^+$-NPs induce functional neuronal differentiation *via* nuclear RAR activation. (A) Composition and physical properties of RA$^+$-NPs. SVZ cells were exposed for 7 days to 100 ng/mL RA$^+$-NPs and/or to the inverse agonist BMS493 (2 μM). (B) Percentage of NeuN-immunostained neurons as a percentage of the total number of cells. Data are expressed as mean ± SEM (n = 16). $^{**,\#\#}$ $P < 0.01$ using Bonferroni's multiple comparison test. (C) Percentage of neuronal-like responding cells (Hist/KCl below 0.8). Data are expressed as mean ± SEM (n = 17). $^{***,\#\#\#}$ $P < 0.001$ using Bonferroni's multiple comparison test.

or mouse teratocarcinoma.[17,18] Regardless of its referred effects, RA is rapidly metabolized by cells, has low solubility in aqueous solutions, and requires a fine-tuning of concentration window to achieve its results,[19] posing difficulties in the delivery of therapeutic doses.

Nanoparticles (NPs) can be a powerful strategy to overcome these limitations by ensuring controlled release of RA. Recently, we reported that the intracellular delivery of retinoic acid-loaded NPs (RA$^+$-NPs) was effective in driving the neuronal differentiation of SVZ neural stem cells *in vitro*.[20] However, it was unclear the molecular mechanism of RA following intracellular delivery and the *in vivo* proneurogenic potential of the formulation was not demonstrated. Here, we show that RA reduces SVZ cell self-renewal while inducing the expression of proneurogenic genes and functional neuronal differentiation *in vitro*. Importantly, RA$^+$-NPs injected in the brain of an animal model contribute for the successful commitment of neural stem cells present in the SVZ niche toward neuronal progenitors expressing Mash1 and Neurogenin1 (Ngn1). The NP formulation described herein is very promising to drive the neuronal commitment of SVZ neural stem cells both *in vitro* and *in vivo* and offers new opportunities to treat neurodegenerative diseases.

RESULTS AND DISCUSSION

RA$^+$-NPs Induce Neuronal Differentiation *via* Nuclear RAR Activation. NPs were prepared by the electrostatic interaction of polyethylenimine (PEI, polycation) complexed with RA and dextran sulfate (DS, polyanion) according to a methodology reported previously by us.[20] RA$^+$-NPs have a DS/PEI ratio of 0.2, yielding NPs that are approximately 220 nm in diameter and have a positive net charge (zeta potential of ~16 mV) (Figure 1A). NPs conjugated with fluorescein isothiocyanate (FITC) (10 μg/mL) are internalized by SVZ cells after exposure for 18 h and accumulate in cell cytoplasm, as confirmed by hyperspectral imaging system (CytoViva) analyses (Supporting Information, Figure 1).

Several reports have suggested the involvement of RA in the modulation of both neural plasticity and neurogenesis in the adult brain (reviewed in ref 7). This process is mediated by the interaction of RA with its receptors.[14] For that reason, we evaluated whether RA delivered intracellularly by RA$^+$-NPs was acting *via* its functional receptor, RAR, in the process of neuronal differentiation. For this purpose, SVZ cells were cultured in differentiation conditions for 7 days, in the presence of 100 ng/mL RA$^+$-NPs. At this concentration, NPs have no cytotoxic effect.[20] As shown in Figure 1B, 100 ng/mL RA$^+$-NPs increased significantly the number of NeuN-positive mature neurons and this proneurogenic effect was completely prevented by 2 μM BMS493, an inverse agonist of the nuclear RARs. BMS493 binding induces analogous conformational changes in all three RARs subtypes, inhibiting their action.[21] Next, we evaluated the functionality of the new differentiated neuronal cells by single cell calcium imaging (SCCI) analysis. For that purpose, we measured the variations of intracellular calcium concentration ($[Ca^{2+}]_i$) in single SVZ cells, following KCl and histamine (Hist)

stimulations, being Hist/KCl ratios below 0.8 characteristic of SVZ-derived neuronal-like cells.[22−24] As shown in Figure 1C, RA^+-NPs induced a significant increase in the percentage of cells presenting Hist/KCl ratios below 0.8 and this effect was also mediated by nuclear RARs activation. An increased expression of β-III tubulin, a microtubule element expressed exclusively in neurons, was also found in RA^+-NPs treated cultures but blocked in cultures cotreated with RA^+-NPs and BMS493 (Supporting Information, Figure 2A). The expression of Glial Fibrillary Acidic Protein (GFAP), an astrocytic marker, was not altered in any experimental condition (Supporting Information, Figure 2B). Importantly, in all experimental settings, BMS493 *per se*, blank nanoparticles (RA^--NPs) or DMSO (at the dilution used to prepare the free RA) had no effect on neuronal differentiation and cell viability (data not shown). Altogether, our results suggest that RA^+-NPs, acting *via* nuclear RARs binding, induce a robust proneurogenic effect in SVZ cell cultures.

RA^+-NPs Sustain Stem/Progenitor Cell Commitment. Adult SVZ neural stem/progenitor cells can divide asymmetrically or symmetrically, either retaining their undifferentiated character or undergoing differentiation, and this decision can be modulated by extrinsic signals.[25] To investigate the effect of RA released from NPs in the asymmetric and symmetric cellular division, single SVZ cells were plated for 24 h in the presence of 4 nM and 10 μM of DMSO-solubilized RA or 100 ng/mL RA^+-NPs. The concentration of 4 nM corresponds to the payload of RA present in 100 ng/mL of RA^+-NPs, whereas 10 μM is the concentration of solubilized RA capable of inducing a proneurogenic effect on SVZ cells *in vitro*.[20] After treatment, the cells where immunostained for Sox2 and Dlx2. Sox2 is a transcription factor expressed in self-renewing and multipotent NSCs,[26] whereas immunodetection of Dlx2 labels SVZ-derived progenitors.[27] Therefore, we quantified the pattern of Sox2 expression in Dlx2-positive cell pairs from SVZ freshly resected cell divisions[28] (Figure 2A). Uncommitted stem/progenitor cells divide symmetrically into two positive NSCs daughter cells (Sox2 +/+), whereas cells committed to differentiate divide asymmetrically into a stem/progenitor and a committed cell (Sox2 +/−), or terminally into two equally committed cells (Sox2 −/−). Noteworthy, after RA^+-NPs exposure, we observed a shift in the type of cell divisions toward terminal symmetric divisions (Sox2 −/−) concomitantly with a significant reduction in the number of Sox2 +/+ cell divisions (Figure 2B). These data indicate that RA^+-NPs increased progenitor cell commitment and reduced NSCs self-renewal capacity. A similar result was obtained with 10 μM RA, however, 4 nM RA was not able to shift cell divisions toward a commited state. A control using DMSO alone also had no effect (data not shown). Further reinforcing these observations, SVZ neurospheres exposed to 100 ng/mL RA^+-NPs generated a lower number of primary neurospheres and less secondary neurospheres as compared to control. Secondary neurospheres were obtained from cells dissociated from the primary neurospheres untreated or treated with RA^+-NPs (Figure 2C). This result is consistent with a loss of self-renewal potentially induced by RA. In summary, our data indicates that RA^+-NPs reduces stemness and direct early immature stem/progenitor cells toward a committed progenitor fate, ultimately leading to late precursors pool expansion and neuronal differentiation. Our results further show that the biological efficacy of RA^+-NPs requires a concentration of 4 nM of encapsulated RA, a concentration that is 100- to 1000-fold lower than the one reported in this study or other studies[14,15] for soluble RA.

RA^+-NPs Promotes Axonogenesis. A newborn neuron must be able to sprout a single axon and multiple neurites in order to integrate a pre-existing neuronal circuitry. SAPK/JNK pathway appears to play an important role in neuronal differentiation and maturation. Indeed, the SAPK/JNK pathway is involved in neurite outgrowth and axonogenesis.[23,24,29] To evaluate the role of RA released by NPs in the activation of SAPK/JNK signaling pathway, the neurospheres were exposed for 6 h to RA^+-NPs and the phosphorylation of SAPK/JNK evaluated by immunocytochemistry. According to Figure 3, RA^+-NPs induced a robust phosphorylation of SAPK/JNK (P-SAPK/JNK: active form) in growth cone-like projections and in axons emerging out of the neurospheres, while control cultures showed a diffuse or faint P-SAPK/JNK staining. Moreover, RA^+-NP treatment increased ~3-fold the total number (Figure 3A) and length (Figure 3B) of P-SAPK/JNK-positive ramifications.

In line with other studies from our group,[23,24] the results obtained with RA^+-NPs also show that P-SAPK/JNK immunoreactivity is colocalizing with Tau, a microtubule-associated protein mainly present in new differentiating axons (Figure 3C). This is consistent with previous studies where nerve growth factor acted *via* RA synthesis to stimulate neurite outgrowth in adult dorsal root ganglia.[16] Therefore, RA^+-NPs are actively involved in the neuronal maturation of SVZ neuroblasts. Altogether, our results suggest that RA^+-NPs promote axonogenesis and axon outgrowth through activation of the SAPK/JNK pathway in Tau-positive axons.

RA Sustains the Expression of the Proneurogenic Genes Mash1 and Ngn1 *In Vitro*. RA induces conformational changes in the nuclear receptors bounded to RARE, causing the dissociation of corepressors and the recruitment of coactivators that comprise histone modifiers, RNA polymerase II, and general transcription factors.[30] Histone modifiers are capable of covalent modifications like acetylation, phosphorylation, and methylation on the N-terminal tails of core histones.[10] Methylation of histone lysine residues is a critical determinant of active and silent gene expression states. Histone 3 trimethylated on lysine 4 (H3K4me3) correlates

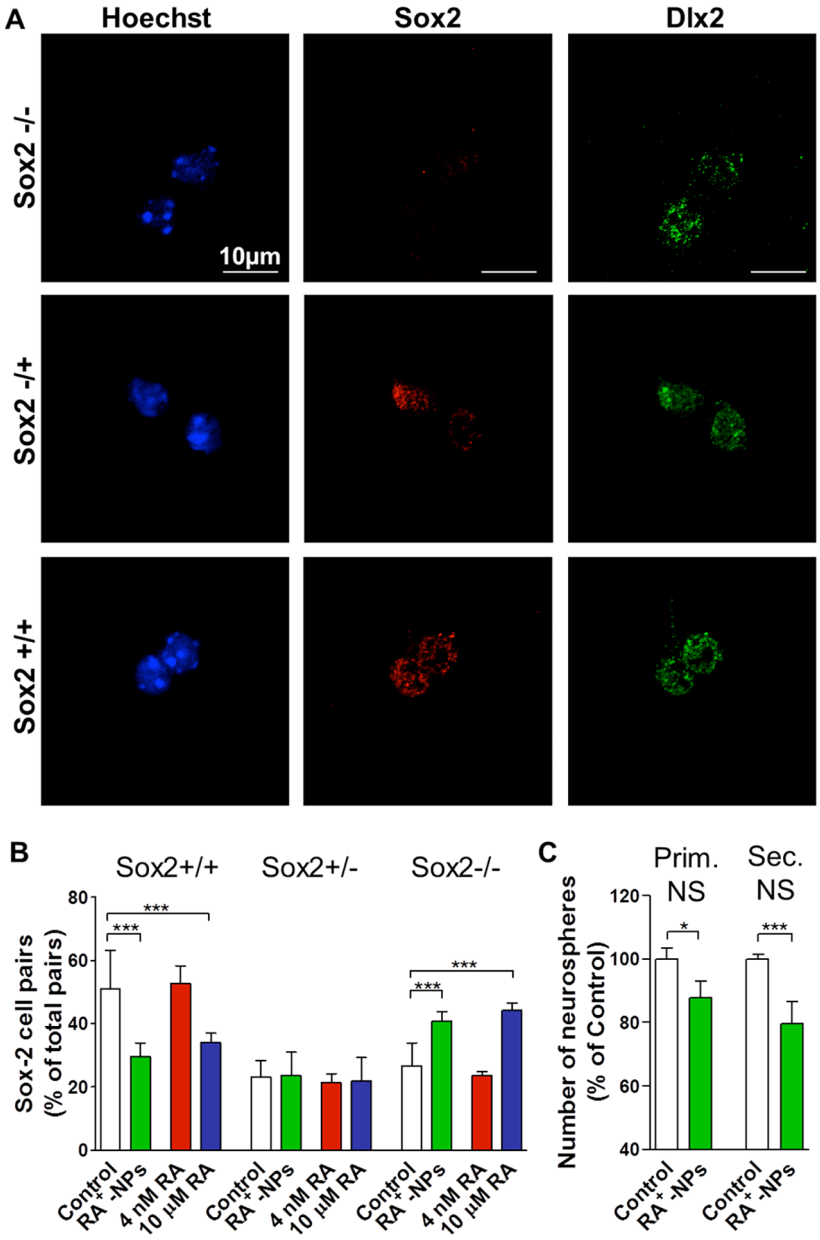

Figure 2. RA$^+$-NPs induce the commitment of SVZ NSCs. (A) Representative confocal digital images of Sox2 −/−, +/−, +/+ cell pairs revealed by Sox2 (red), Dlx2 (green) and Hoechst-33342 (blue) labeling. Scale bars: 10 μm. (B) Bar graph illustrates the percentage of Sox2 +/+, +/−, −/− daughter cells per total cell pairs after incubating SVZ cells with 100 ng/mL RA$^+$-NPs, 4 nM RA, or 10 μM RA for 24 h. Data are expressed as mean ± SEM (n = 10); ***P < 0.001 using Bonferronís multiple comparison test. (C) Bar graph shows the percentage of primary neurospheres (NS) generated upon 100 ng/mL RA$^+$-NPs exposure and the resultant secondary NS cultured in untreated medium. Control values were normalized to 100%. Data are expressed as mean ± SEM (n = 8); *P < 0.05 and ***P < 0.001 using paired Student's t test.

strongly with active transcription.[31,32] Therefore, we performed quantitative chromatin immunoprecipitation (qChIP) studies to monitor the presence of H3K4me3 at Mash1 and Neurogenin1 (Ngn1) promoter regions. Mash1 (also recognized as Ascl1) and Ngn1 are two basic helix−loop−helix (bHLH) proteins that are strongly associated with neuronal differentiation.[18,33] Basic helix−loop−helix (bHLH) proteins exist in most stages of neural lineage, which play crucial roles in determining cell fates and are essential in neurogenesis.[34] Accordingly, we observed an increase of H3K4me3 recruitment to Mash1 promoter one day after RA$^+$-NPs treatment (Figure 4A), whereas the enhancement of H3K4me3 associated with the Ngn1 promoter region was only detected the second day after treatment (Figure 4A). These observations suggested that RA$^+$-NPs treatment enhances the transcriptional activity of Mash1 and Ngn1 promoters, thus, we further examined Mash1 and Ngn1 mRNA expression through quantitative RT-PCR (qRT-PCR). In line with qChIP results, Mash1 and Ngn1 mRNA levels were increased three days after cell treatment with 100 ng/mL RA$^+$-NPs

(Figure 4B,C). Surprisingly, solubilized RA at 10 μM increased Ngn1 mRNA levels but was not able to increase the expression of Mash1. As expected, 4 nM RA was not able to induce an overexpression of both proneurogenic genes (Figure 4B). The expression of both Mash1 and Ngn1 genes was also evaluated 2 days after cell treatment; however, no effect was observed in all conditions tested (data not shown).

The epigenetics behind RA-induced neuronal differentiation seems to be different between free RA and RA$^+$-NPs. NSCs are a heterogeneous population of cells comprising immature multipotent cells and commited progenitors which have a variable epigenetic signature and genetic profile.[35] For example, Mash1 is expressed predominantly in transit amplifying C cells (GFAP-Nestin+EGFR+Ki67+) but also in a small subset of slow-dividing B stem cells (GFAP+Nestin+).[36−38] Moreover, Ngn1 is higly expressed in proliferating progenitors undergoing late cell divisions.[39] Based on this data, we postulate that RA$^+$-NPs may be targeting a broader population of cells than free RA. Moreover, it cannot be excluded that the intracellular machinery involved in the Mash1 and Ngn1 expression may respond differently to the continuous release of RA by the RA$^+$-NPs versus one-pulse treatment of free RA. Thus, SVZ cells may be differentially responsive to distinct platforms of RA delivery (NPs vs free RA), ultimately resulting in distinct dynamics of gene expression.

Altogether, our data suggest that RA$^+$-NPs increases the commitment of mouse SVZ cells to the neuronal lineage by epigenetic modifications and the subsequent mRNA expression of proneurogenic genes such as Ngn1 and Mash1. Our results agree with previous results showing that RA promotes proliferation and neuronal commitment of P19 cells through epigenetic regulation of the Ngn1 expression.[18] Furthermore, our results corroborate previous findings, highlighting the importance of Mash1 expression in neurogenesis.[40]

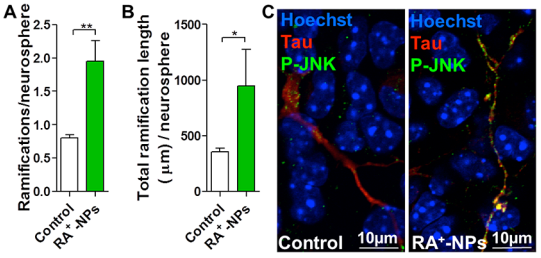

Figure 3. RA$^+$-NPs activate the SAPK/JNK pathway in Tau-positive axons. Bar graphs depict (A) the number of ramifications and (B) the total length (μm) of ramifications *per* neurosphere. Data are expressed as a mean ± SEM (n = 3); *P < 0.05, **P < 0.01, using paired Student's t test. (C) Representative confocal digital images of the P-SAPK/JNK (green), Tau (red), and Hoechst 33342 staining (blue) in control cultures and in cultures exposed to 100 ng/mL RA$^+$-NP for 6 h. Double-labeling of P-SAPK-JNK and Tau in growth cone-like structures and axons was seen in RA$^+$-NP treated cultures. Scale bars are 10 μm.

RA$^+$-NPs Modulate the Expression of Proneurogenic Genes in the *In Vivo* SVZ Neurogenic Niche. Next, we demonstrated the proneurogenic potential of RA$^+$-NPs *in vivo*, at the SVZ cell niche. We delivered the RA$^+$-NPs intracerebroventricularly (i.c.v.), directly into the ventricular lumen by using a stereotaxic apparatus. As shown in Figure 5A, internalized FITC-labeled RA$^+$-NPs were easily detected, lining the lateral ventricle (LV) in the SVZ of treated mice but not in saline-injected animals. Later on, we collected the SVZ by laser microdissection (Figure 5B) and the mRNA levels of Mash1 and Ngn1 were quantified by qRT-PCR. These genes were selected because their expression in the SVZ is residual under normal conditions[37,41] and, thus, facilitate the monitoring of differentiation induced by the RA. It has been demonstrated that the expression of Mash1 is sufficient to induce neuronal differentiation.[42−44]

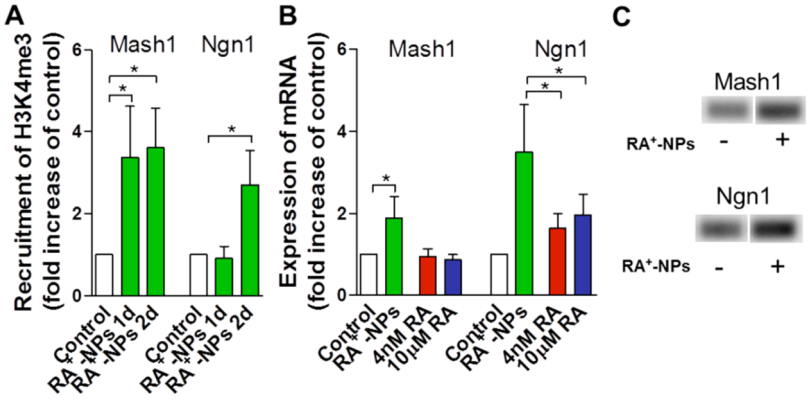

Figure 4. RA$^+$-NPs promote the expression of proneurogenic genes *in vitro*. (A) Bar graphs show the fold increase of H3K4me3 associated with the promoter regions of Mash1 and Ngn1 assessed by qChIP and (B) the fold increase of the respective mRNA expression for both genes, measured by qRT-PCR, in control, 100 ng/mL RA$^+$-NPs, 4 nM RA, and 10 μM RA-treated cell cultures for 1 and 2 days (qChIP) or 3 days (qRT-PCR). Data are expressed as fold increase relative to control (set to 1), mean ± SEM (n = 5−7); *P < 0.05 using Bonferroni's multiple comparison test. (C) Representative agarose gel for Mash1 and Ngn1 qRT-PCR amplicons in control (−) and RA$^+$-NPs treated (+) cells for 3 days.

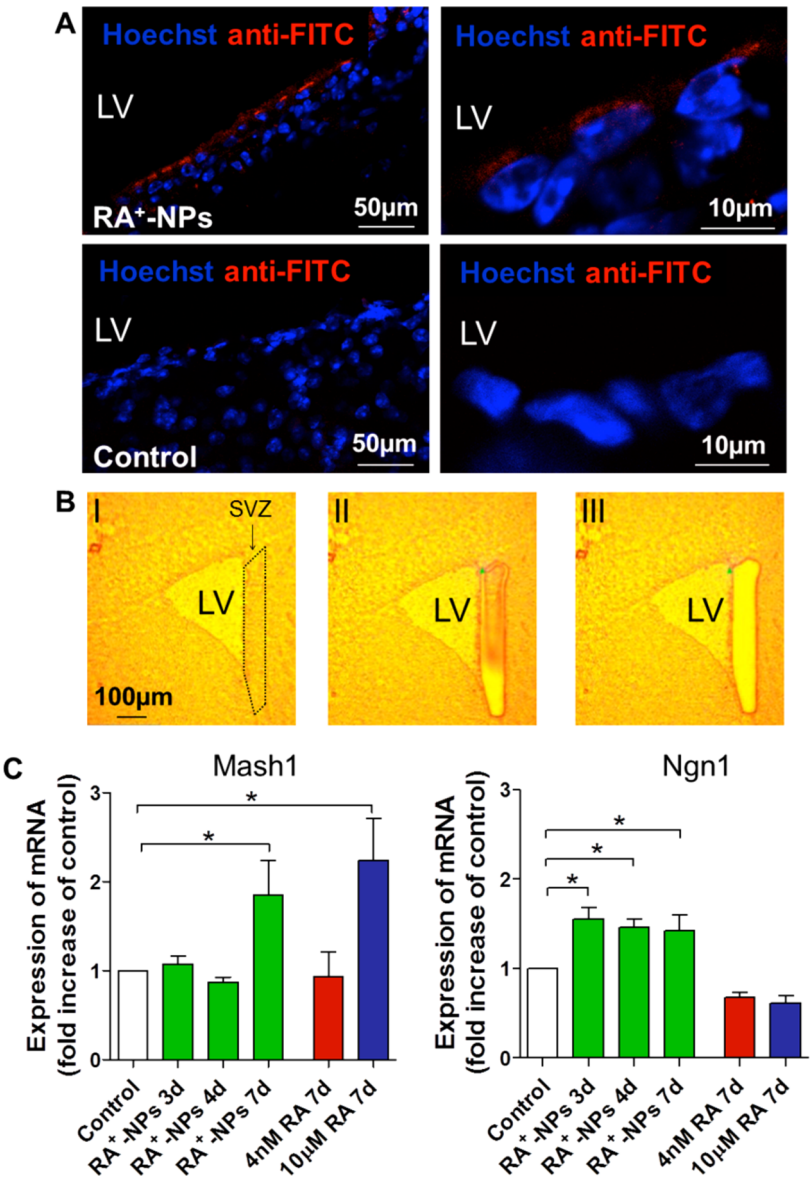

Figure 5. RA^+-NPs induce the expression of proneurogenic genes in the SVZ neurogenic niche *in vivo*. (A) Confocal digital images indicating the presence of FITC-labeled RA^+-NPs (red) lining the lateral ventricles 1 day after i.c.v. injection with RA^+-NPs, but not in saline-injected animals (control). Fluorescent pictures at the right side are magnifications of figures on the left side. Scale bars are 50 and 10 μm. (B) Representative digital images of the laser microdissection procedure depicting a mouse brain slice at the levels of the lateral ventricle; I: Identification of the SVZ region; II: SVZ was circumscribed and separated from unwanted cells; III: Laser shots catapulted the SVZ tissue into a lid of a PCR tube. Scale bar: 100 μm. (C) Bar graphs indicate the fold increase of mRNA expression for Mash1 and Ngn1, measured by qRT-PCR, in control, 100 ng/mL RA^+-NPs, 4 nM RA and 10 μM RA-treated animals for 3, 4, or 7 days after i.c.v. injection. Data are expressed as fold increase relative to control (set to 1), mean $\pm$ SEM ($n = 5-10$); *$P < 0.05$ using Bonferroni's multiple comparison test.

Similar to the *in vitro* results, the SVZ in animals treated with RA^+-NPs express Mash1 and Ngn1. However, Mash1 and Ngn1 revealed different timings of expression: Mash1 mRNA levels only increased after 7 days postinjection, while Ngn1 mRNA levels increased after 3 days and were maintained up to 7 days after injection (Figure 5C). No differences were detected between animals injected with RA^--NPs, saline or DMSO (data not shown). The differences in the *in vitro* and *in vivo* kinetics might be ascribed to differences in the cellular composition found in the *in vivo* and *in vitro* SVZ cells. *In vitro*, SVZ cells' progeny is mostly derived from the highly mitotic transit-amplifying C cells and not quiescent stem cells such as type B stem cells (Figure 6). The cells exposed to epidermal growth factor (EGF) grow to form neurospheres that are multipotent and self-renewing.[27] *In vivo*, SVZ cells' progeny is derived from quiescent stem cells type B that give origin to rapidly dividing transit-amplifying C cells, which ultimately generate newly born neurons (Figure 6). These stem cells expand a cilium through the monolayer of ependymal layer surrounding the ventricles in order to contact the

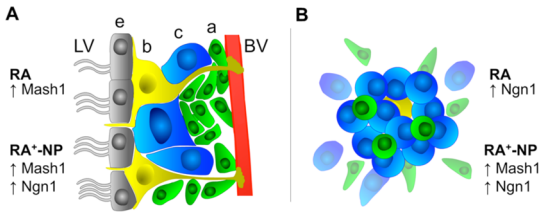

Figure 6. Dynamics of initial stages of differentiation between SVZ cells treated with RA$^+$-NPs and solubilized RA. (A) *In vivo*, the SVZ contains a subpopulation of neural stem cells, or type B cells (b; yellow), that contact with ependymal cells (e; gray), the ventricular lumen and blood vessels (BV; red). Type B cells give origin to rapidly dividing transit-amplifying C cells (c; blue), which in turn generate neuroblasts or type A cells (a; green). These neuroblasts will ultimately differentiate into mature neurons. Upon i.c.v. injection with solubilized RA or RA$^+$-NPs, the SVZ population overexpresses Mash1 and Mash1/Ngn1, respectively. (B) *In vitro*, SVZ cells form neurospheres, mainly composed by EGF-responsive type C cells (blue). Under differentiation conditions, neurospheres give rise to a mixed population of progenitors in different stages of differentiation, neurons, oligodendrocytes, and astrocytes. Upon treatment with solubilized RA or RA$^+$-NPs, the SVZ population overexpresses Ngn1 and Mash1/Ngn1, respectively.

cerebrospinal fluid (CSF).[45] Therefore, RA$^+$-NPs can affect the neurogenic microenvironment by the contact with ependymal cells (paracrine effect) or by the direct contact with the cilium displayed by SVZ GFAP-positive stem cells (type B cells) that contact the ventricles lumen. It should be noted that differences in gene expression of SVZ cells *in vivo* and *in vitro* (neurospheres) have been also described in the setting of stroke.[46] These changes end up being complementary, but they are not the same. Seven days after stroke, only 8 out of the 23 genes upregulated *in vitro* were also upregulated *in vivo*.[46]

The delivery of high (10 μM), but not low (4 nM), concentrations of soluble RA in the *in vivo* ventricular lumen had a different impact in gene expression than *in vitro*. In line with the *in vitro* results, 4 nM RA was ineffective in inducing the *in vivo* expression of Mash1 and Ngn1 (Figure 5C). However, in contrast with the *in vitro* results, 10 μM RA induced a robust increase in the expression of Mash1, 7 days postinjection, but had no effect on Ngn1 mRNA levels, either after 3 or 7 days (data not shown). The results highlight differences in the differentiation dynamics of the SVZ cells either *in vivo* or *in vitro* likely because of their intrinsic composition (see above). Furthermore, the fact that the CSF is being constantly filtered and renewed by the *choroid plexus*,[47] it is possible that this could interfere with the free RA injected. Therefore, it is likely that cells were exposed to different times of RA both *in vitro* and *in vivo*.

Overall, our results indicate that the dynamics of differentiation are clearly different *in vitro* and *in vivo* for SVZ cells treated with RA$^+$-NPs and solubilized RA. The differences are likely ascribed to differences in composition of SVZ cells *in vivo* and *in vitro*, but also in differences related to the uptake and intracellular delivery of RA when it is solubilized or encapsulated in a NP formulation. Our results further indicate that RA$^+$-NPs are more efficient to differentiate the SVZ cells than solubilized RA because a less amount of RA is needed (4 nM versus 10 μM). The results present here launch the foundations for the use of nanomaterials to control the *in vivo* stem cell niches.

CONCLUSIONS

In conclusion, this work reports three important findings. First, we demonstrate the differentiation mechanism mediated by RA released from a polymeric NP within neural stem cells. NPs were used to facilitate the cellular internalization, intracellular positioning, and concentration of RA above its solubility limit (approximatelly 63 ng/mL) at physiologic pH.[19] Our results show that RA released from NPs interacted with RA receptor (RAR), activated SAPK/JNK signaling pathway, and induced the methylation of histone lysine residues that, in turn, associated with the promoter regions of proneurogenic genes such as Ngn1 and Mash1. Second, we demonstrated successfully that a NP formulation could be used *in vivo* to control the differentiation of neural stem cells. Although a previous study has shown that NP formulations may be an efficient platform to transfect SVZ cells *in vivo* with plasmid DNA expressing the nucleus-targeting fibroblast growth factor receptor type 1,[48] to the best of our knowledge, no study has demonstrated so far the ability of controlling *in vivo* the neuronal differentiation of SVZ cells by small molecules delivered from NPs. Notably, our formulation offers a significant advantage over free solubilized RA, either by avoiding the use of solvents like DMSO or by achieving a proneurogenic effect with a RA concentration ~2500-fold lower than the one needed with free RA. Third, our study is the first to show the dynamics of the initial stages of stem cell differentiation either *in vitro* or *in vivo* after exposure to a formulation of NPs containing a biomolecule or a solubilized biomolecule. The study of the differentiation profile of stem cells in both conditions is important to design more effective formulations to modulate the stem cell niche. Our results show that RA$^+$-NPs were more robust in maintaining the signature of gene expression (although with different kinetics) either *in vitro* or *in vivo* than solubilized RA (Figure 6). Although not explored, the NP formulation described herein can be engineered at surface level to display stem cell targeting sequences to maximize its location and effect. Following the recent advances in the use of RA to treat Alzheimer's disease,[49] hippocampal memory deficits,[50] and stroke,[51] our results provide

foundations for the use of RA^+-NPs to modulate *in vivo* the differentiation of neural stem cells and open new perspectives for the treatment of neurodegenerative diseases.

MATERIALS AND METHODS

All experiments were performed in accordance with NIH and European Community Council Directives (86/609/EEC) guidelines and the Portuguese law for the care and use of laboratory animals (DL No. 129/92).

SVZ Cell Cultures and Experimental Treatments. SVZ cells were prepared from 1−3-day-old C57BL/6 donor mice, as described by Agasse and Bernardino *et al.* (2008).[22] Briefly, mice were sacrificed by decapitation and the brains were removed and placed in calcium- and magnesium-free HBSS solution supplemented with 100 U/mL penicillin and 100 μg/mL streptomycin (all from Invitrogen, Carlsbad, CA, U.S.A.) under sterile conditions. Fragments of SVZ were dissected out of 450 μm thick coronal brain sections using a McIlwain tissue chopper, and then SVZ was digested in 0.025% trypsin, 0.265 mM EDTA (all from Invitrogen; 10 min, 37 °C), followed by mechanical dissociation with a P1000 pipet. The cell suspension was diluted in serum-free medium (SFM) composed of Dulbecco's modified Eagle medium [(DMEM)/F12 + GlutaMAX-I)] supplemented with 100 U/mL penicillin, 100 μg/mL streptomycin, 1% B27 supplement, 10 ng/mL epidermal growth factor (EGF), and 5 ng/mL basic fibroblast growth factor-2 (FGF)-2 (all from Invitrogen). Single cells were then plated on uncoated Petri dishes at a density of 3000 cells/cm^2 and allowed to develop in an incubator with 5% CO_2 and 95% atmospheric air, at 37 °C.

Six-day-old neurospheres were adhered for 2 days onto poly-D-lysine (0.1 mg/mL)-coated glass coverslips, in 24-well plates, for all experiments except Western blots, qChIP, and qRT-PCR, which were left adherent onto poly-D-lysine (0.1 mg/mL)-coated 6-well plates, in growth factor-devoid SFM. Then, the neurospheres were allowed to develop for different time frames in the presence of RA^+-NP (100 ng/mL), blank nanoparticles (void nanoparticles; RA^--NP; 100 ng/mL), or free RA (4 nM or 10 μM). Controls, including the respective dilution of DMSO used to prepare the free RA (dilutions 1:25000000 and 1:10000), were also included in the experimental setup.

Preparation of Nanoparticles. Nanoparticles were prepared by adding dropwise 0.6 mL of RA (2% w/v, in DMSO) into 12 mL of PEI (1% w/v, in pH 8.0 borate buffer). The formation of complexes between RA-PEI occurred immediately and was allowed to proceed for 30 min with intense magnetic stirring. Then, 2.4 mL of DS solution (1% w/v) was added dropwise and stirred for another 5 min. Finally, 1.2 mL of $ZnSO_4$ aqueous solution (1 M) was added and stirred for 30 min. Nanoparticles were centrifuged three times in 5% mannitol solution at 14000 g for 20 min. Supernatants from each step were collected to determine PEI and DS amounts in nanoparticles. Resulting nanoparticles were frozen and lyophilized for 4 days to obtain a dry powder. Lyophilized nanoparticles were stored at 4 °C. Blank nanoparticles were prepared using the same procedure in the absence of RA.

Hyperspectral Scan from CytoViva. The Hyperspectral imaging system from CytoViva (CytoViva Inc., Auburn, AL) was used to identify the presence of RA^+-NPs within SVZ cell cytoplasm. The CytoViva hyperspectral imager captures the unique reflectance spectra for each high resolution image pixel (down to 64 nm), enabling data to be presented as a spectral curve and RGB image. First, an aqueous suspension of FITC-conjugated RA^+-NPs was hyperspectral scanned in order to generate a reference spectra library. The emitted spectra signatures were collected within each pixel of the scanned field, enabling pixel level spectra quantification of the sample. Then the reference spectra was compared to those obtained in cells treated for 18 h with 10 μg/mL of RA^+-NPs or untreated cells (control). On our untreated sample, no RA^+-NPs spectra was mapped (data not shown).

Pharmacological Treatments. To investigate the influence of retinoic acid on neuronal differentiation, SVZ cells were exposed to 100 ng/mL of RA^+-NPs or 4 nM or 10 μM free RA for 7 days.[20] Controls, including void RA^--NPs nanoparticles and DMSO, were also performed. To disclose the involvement of retinoic acid receptors in the proneurogenic effect exerted by RA^+-NPs, cultures were coexposed with RA^+-NPs and 2 μM BMS493 (inverse pan-RAR agonist; Tocris, Missouri, U.S.A.) for 7 days. BMS493 treatment was renewed every 2 days.

In experiments concerning the involvement of the JNK/MAPK signaling pathway, SVZ cells were exposed to 100 ng/mL RA^+-NPs for 6 h.

To assess whether RA^+-NPs promotes the recruitment of H3K4me3 on the promoter region of Mash1 and Ngn1, cells were incubated with 100 ng/mL RA^+-NPs for 1 and 2 days and then processed for qChIP. To confirm qChIP analysis, mRNA expression levels of the above-mentioned genes were determined by qRT-PCR at 2 and 3 days.

Single Cell Calcium Imaging. SVZ cultures treated for 7 days with 100 ng/mL RA^+-NPs were loaded for 40 min at 37 °C with 5 μM Fura-2 AM (Invitrogen), 0.1% fatty acid-free bovine serum albumin (BSA), and 0.02% pluronic acid F-127, in Krebs buffer (132 mM NaCl, 1 mM KCl, 1 mM $MgCl_2$, 2.5 mM $CaCl_2$, 10 mM glucose, 10 mM HEPES, pH 7.4). After a 10 min postloading period at room temperature (RT), the coverslips were mounted on a RC-25 chamber in a PH3 platform (Warner Instruments, Hamden, CT, U.S.A.) on the stage of an inverted Axiovert 200 fluorescence microscope (Carl Zeiss, Göttingen, Germany). Cells (approximately 100 cells per field) were continuously perfused with Krebs and stimulated by applying 100 μM histamine or high-potassium Krebs solution (containing 50 mM KCl, isosmotic substitution with NaCl) by the mean of a fast pressurized (95% air, 5% CO_2 atmosphere) system (AutoMate Scientific Inc., Berkeley, CA, U.S.A.). $[Ca^{2+}]_i$ was evaluated by quantifying the ratio of the fluorescence emitted at 510 nm following alternate excitation (750 ms) at 340 and 380 nm, using a Lambda DG4 apparatus (Sutter Instrument, Novato, CA, U.S.A.) and a 510 nm long-pass filter (Carl Zeiss) before fluorescence acquisition with a 40× objective and a CoolSNAP digital camera (Roper Scientific, Tucson, AZ, U.S.A.). Acquired values were processed using the MetaFluor software (Universal Imaging, Downingtown, PA, U.S.A.). KCl and histamine peaks given by the normalized ratios of fluorescence at 340/380 nm were used to calculate the Fura-2 ratios of response to histamine/KCl. The percentage of cells displaying a neuronal-like profile was calculated on the basis of the histamine/KCl ratio.[22]

Western Blots. SVZ cells, previously incubated with 100 ng/mL RA^+-NPs, for 7 days, in differentiation conditions, were washed with 0.15 M phosphate-buffered saline (PBS) and incubated in a lysis buffer [0.15 M NaCl, 0.05 M Tris-Base, 5 mM EGTA, 1% Triton X-100, 0.5% DOC, 0.1% SDS, and 10 mM DTT containing a cocktail of proteinase inhibitors (Roche, Basel, Switzerland)]. Total protein concentration from the lysates was determined by BCA assay and samples were treated with SDS-PAGE buffer [6× concentrated: 350 mM Tris, 10% (w/v) SDS, 30% (v/v) glycerol, 0.6 M DTT, 0.06% (w/v) bromophenol blue], boiled for 5 min at 95 °C, and stored at −20 °C until use for Western blotting. Then, proteins (40 μg of total protein) were resolved in 12% SDS polyacrilamide gels and then transferred to PVDF membranes with 0.45 μm pore size in the following conditions: 300 mA, 90 min at 4 °C in a solution containing 10 mM CAPS and 20% methanol, pH 11). Membranes were blocked in Tris-buffer saline containing 5% low-fat milk and 0.1% Tween 20 (Sigma, St. Louis, MO, U.S.A.) for 1 h, at RT, and then incubated overnight at 4 °C with mouse monoclonal anti-βIII-tubulin (1:1000; Cell Signaling, Beverly, MA, U.S.A.) or rabbit monoclonal anti-GFAP (1:20000; Sigma) antibodies, both diluted in 1% TBS-Tween and 0.5% low fat milk. After rinsing three times with TBS-T containing 0.5% low-fat milk, membranes were incubated for 1 h, at RT, with an alkaline phosphatase-linked secondary antibody antimouse IgG 1:20000 or antirabbit IgG 1:20000 in 1% TBS-T and 0.5% low-fat milk (both from GE

Healthcare, Buckinghamshire, U.K.). For endogenous control immunolabeling, primary antibody solution consisted of mouse monoclonal anti-β-actin (1:20000; Sigma). Protein immunoreactive bands were visualized in a Versa-Doc Imaging System (Model 3000, BioRad Laboratories, CA, U.S.A.), following incubation of the membrane with ECF reagent (GE Healthcare) for 5 min. Densitometric analysis were performed using the Quantity one software (BioRad).

Immunocytochemistry. Cells were fixed with 4% paraformaldehyde (PFA). After washing three times with PBS, unspecific binding was prevented and cells were permeabilized by incubation with a 3% BSA and 0.3% Triton X-100 solution for 30 min, at RT. Cells were kept overnight at 4 °C in a primary antibody solution, then washed with PBS the following day, and incubated for 1 h, at RT, with the corresponding secondary antibody. Primary antibodies were used as listed: rabbit monoclonal anti-Phospho-JNK (1:100; Cell Signaling), mouse polyclonal anti-Tau (1:200; Cell Signaling), rabbit polyclonal anti-Dlx2 (1:200; Abcam, Cambridge, U.K.), goat polyclonal anti-Sox2 (1:700; Santa Cruz Biotechnology, Santa Cruz, CA, U.S.A.), mouse monoclonal anti-FITC (1:100; Sigma), mouse monoclonal anti-NeuN (1:100; Millipore), all prepared in 0.1% Triton X-100 and 0.3% BSA solution; secondary antibodies were as follows: Alexa Fluor 594 donkey antimouse, rabbit or goat, Alexa Fluor 488 donkey antimouse or rabbit (all at 1:200 in PBS, from Invitrogen). For nuclear labeling, cell preparations were stained with Hoechst 33342 (2 μg/mL; Invitrogen) in PBS for 5 min, at RT, and mounted in Dako fluorescent medium (Dakocytomation Inc., Carpinteria, CA, U.S.A.). Fluorescent images were acquired using a confocal microscope (LSM 510 Meta, Carl Zeiss).

Sox2 Cell Pair Assay. Dissociated SVZ cell suspension obtained from freshly dissected SVZ explants were plated onto poly-D-lysine coated glass coverslips at a density of 6400 cells/cm^2. After seeding, SVZ cells were grown in SFM containing 5 ng/mL EGF and 2.5 ng/mL FGF-2 (low EGF/FGF-2) supplemented or not (control) with 100 ng/mL RA$^+$-NPs, 4 nM or 10 μM RA, for 24 h. Cells were then fixed in ice cold methanol for 15 min at −20 °C and processed for immunocytochemistry against Sox2 and Dlx2.

Self-Renewal Assay. SVZ cells were seeded at 2500 cells *per* well in 24-well cell culture plates in SFM containing low EGF/FGF-2 and supplemented or not (control) with 100 ng/mL RA$^+$-NPs. After 6 days, the number of primary neurospheres was determined. Then, the neurospheres were collected, dissociated as single cells (Neurocult dissociation kit, Stem Cell Technology, Grenoble, France) and seeded in low EGF/FGF-2 medium without any treatment. After 6 days, the number of secondary neurospheres was determined. Data was obtained from counting the number of primary and secondary neurospheres in each well, in quadruplicate, *per* independent cell culture.

Quantitative Chromatin Immunoprecipitation (qChIP). After treatment of SVZ cells with 100 ng/mL RA$^+$-NPs for 1 and 2 days, cells were washed with 0.15 M PBS, and the chromatin was cross-linked to proteins by incubating cells with 1% formaldehyde in PBS containing 50 mM $MgCl_2$, for 15 min, at 37 °C. SVZ cells were then incubated with 125 mM glycine, for 10 min at RT, washed twice with sterile 0.15 M PBS, and incubated with lysis buffer [1% SDS, 10 mM EDTA, 50 mM Tris pH 8.1, containing a cocktail of proteinase inhibitors (Roche)], for 5 min. Samples were sonicated repeatedly on ice [using Sonics and Materials, Model Vibra Cell (TM) VC 50; Parameters: power 20, time 10 × 30 s with 30 s intervals, on ice)], to cleave genomic DNA. After the analysis of the genomic DNA fragments in a 1% agarose gel, cell suspension was centrifuged at 10000 g, for 5 min, at 4 °C. The supernatant was diluted 10-fold in ice-cold dilution buffer [0.01% SDS, 1% Triton, 1.2 mM EDTA, 16.7 mM Tris pH 8.1, 167 mM NaCl, and a cocktail of protease inhibitors (Roche)]. Then, samples were precleared with 30 μL of 50% blocked protein G-sepharose beads (Sigma) in 0.15 M PBS, for 30 min at 4 °C, with rotation. Beads were afterward eliminated by centrifugation at 10000 g, for 5 min, at 4 °C. While 1/10 was kept as the input, the remaining portion, for each sample, was incubated with 10 μg mouse monoclonal antibody against Histone H3 trimethylated on lysine 4 (H3K4me3, Abcam), at 4 °C, overnight. A negative control was done by incubating half of the respective sample with 10 μg of an unrelated antibody (rabbit polyclonal anti-TNFR1, Santa Cruz Biotechnology). Immune complexes were captured by 1 h incubation with 40 μL of 50% blocked protein G sepharose beads, at 4 °C. Then, protein G-sepharose beads were rinsed 7 times, for 10 min, in washing buffer (TE containing 150 mM NaCl and 0.5% NP40) and incubated with 50 μg/mL RNaseA/TE, for 30 min, at 37 °C. The input-lysate was prepared in the same way. Proteinase K (1 mg/mL) and SDS (0.5%) were added to samples that were left overnight at 37 °C, before being incubated at 65 °C for 3 h for reverse cross-linking. After a centrifugation at 1000 g, for 5 min, beads were discarded and the DNA samples were purified by phenol−chloroform extraction and precipitated with 1 μg glycogen, plus sodium acetate and ethanol. The DNA pellets were suspended in nuclease-free water and DNA was then subjected to qPCR analysis with SybrGreen (iQ SYBR Green Supermix; BioRad).

For gene expression analysis, 2 μL of sample DNA or 1 μL of the respective input were added to 10 μL SYBR Green Supermix, and the final concentration of each primer was 0.2 μM in 20 μL total volume. The thermocycling reaction was initiated with activation of Taq DNA polymerase by heating at 95 °C during 3 min, followed by 40 cycles of a 10 s denaturation step at 95 °C and a 30 s annealing and elongation step at 64 °C. The fluorescence was measured after the extension step by the iQ5-Multicolor Real-Time PCR Detection System (Biorad). After the thermocycling reaction, a melting curve was performed with slow heating, starting at 55 °C and with a rate of 0.5 °C per 10 s, up to 95 °C, with continuous measurement of fluorescence, allowing detection of possible nonspecific products. The assay included a nontemplate control (sample was substituted by RNase- DNase-free sterile water) and a standard curve (in 10-fold steps) of DNA for assessing the efficiency of each set of primers. All reactions were run in duplicates. Primers used in real-time analysis were as follows: GAPDH: forward primer 5′-CAA GGC TGT GGG CAA GGT-3′ and reverse primer 5′-TCA CCA CCT TCT TGA TGT CAT CA-3′;[33] Mash1: forward primer 5′-CCC TGG CCA GAA GTG AGA-3′and reverse primer 5′-CTG GGT GTC CCA TTG AAA AG-3′; Neurogenin1 (Ngn1) forward primer 5′-ATT ACG GGC ACG CTC CAG-3′, reverse primer 5′-CAG CTC CTG TGA GCA CCA AG-3′.[18] The threshold cycle (Ct) was measured in the exponential phase and therefore was not affected by possible limiting components in the reaction. Data analysis was performed with BioRad iQ5 software. Recovery of genomic DNA as a percentage input was calculated as the ratio of copy numbers in the precipitated immune complexes to the input control. The relative expression of each gene was normalized against GAPDH.

cDNA Synthesis and Quantitative RT-PCR Analysis. For cDNA synthesis, 1 μg of total RNA was mixed with 2.5 μM anchored-oligo-p(dT)18 primers, 1× PCR reaction buffer, 20 U RNase inhibitor, dNTPs (1 mM each), and 10 U AMV reverse transcriptase in a 20 μL final volume (Roche). The reaction was performed at 55 °C for 30 min and stopped by 85 °C for 5 min step. The samples were then stored at −80 °C until further use. For gene expression analysis, 2 μL of sample cDNA were added to 10 μL of Evagreen Supermix (SsoFast Evagreen Supermix, Biorad), and the final concentration of each primer was 1/10 of total volume according to primers datasheet. The thermocycling reaction was initiated with activation of Taq DNA polymerase by heating at 94 °C during 3 min, followed by 40 cycles of a 15 s denaturation step at 94 °C, and a 30 s annealing and elongation step at 60 °C for Mash1 and 64 °C for Ngn1. Validated primer sets for use in real-time RT-PCR were obtained from selected QuantiTect Primer Assays (Qiagen, Austin, Texas). The fluorescence was measured after the extension step by the iQ5Multicolor Real-Time PCR Detection System (Biorad). After the thermocycling reaction, the melting step was performed with slow heating, starting at 55 °C and with a rate of 0.5 °C per 10 s, up to 95 °C, with continuous measurement of fluorescence, allowing detection of possible nonspecific products. The assay included a nontemplate control and a standard curve (in 10-fold steps) of DNA for assessing the efficiency of each set of primers. All reactions were run in duplicates. Ct values were measured in the exponential phase. Data analysis was performed with BioRad iQ5 software (BioRad). The relative expression of each gene was normalized against GAPDH, using the comparative Ct method as described by Pfaffl's formula.[52]

The PCR products were subjected to electrophoresis in a 1% agarose gel stained with ethidium bromide. Photographs were taken in a Gel-Doc Imaging System (BioRad).

***In Vivo* Experiments.** Adult male mice (8−10 weeks old) were anesthetized with intraperitoneal injection of 2,2,2-tribromoethanol (avertin; 240 mg/g of mice weight). After reaching full anesthesia, mice were placed on the stereotaxic frame (Stoelting 51600, Dublin, Ireland). Scalp was disinfected with Betadine and an incision was made along the midline with a scalpel. With the skull exposed, scales were taken after setting the zero at the bregma point (X, AP: +0.70; Y, ML: −0.75; corresponding to the right lateral ventricle). The skull was drilled and the syringe was lowered until the target (Z, DV: −2.85). The intracerebroventricular injection of 100 ng/mL RA^+-NPs (dissolved in 0.15 M PBS) and 4 nM or 10 μM RA (dissolved in DMSO), was performed with a Hamilton syringe at a speed of 0.5 μL/min during 5 min. Controls including RA^--NPs, vehicle (0.15 M PBS), and DMSO were also included in the experimental setup. After the needle was removed and the incision sutured, mice were kept warm during recovery (37 °C). Three, four, or seven days after injection, mice were sacrificed and the brains were removed and frozen with freezer spray (Thermo Scientific, Braunschweig, Germany). Coronal brain sections were cut on a freezing cryostat (−18 °C) at a thickness of 10 μm and mounted on polyethylene naphthalate (PEN)-membrane slides (Carl Zeiss), which were previously treated by UV irradiation for 30 min at 254 nm. After sectioning, the slides were fixed using ethanol 90% (v/v). Laser microdissection and pressure catapulting (LMPC) of SVZ region was carried out using a PALM MicroBeam IP system featuring a 337 nm nitrogen laser (Carl Zeiss) and a 20× LD-PlanNeoFluar objective (Carl Zeiss). A total of 6 mm^2 of tissue sample was collected directly in the cap of microfuge tubes. The same stereotaxic coordinates were always used to circumscribe the SVZ region by LMPC analysis. After LMPC, the tissue sample was immediately processed for mRNA extraction and the protocol followed was as described previously for qRT-PCR analysis.

Immunohistochemistry. To detect the presence of RA^+-NPs in the subventricular zone, intracerebroventricularly injected mice (as described previously) were sacrificed and the brains were removed and frozen with freezer spray (Thermo Scientific). Coronal brain sections were cut on a freezing cryostat (−18 °C) at a thickness of 50 μm and mounted on Superfrost Plus slides (Thermo Scientific). After sectioning, the preparations were fixed in methanol/acetone (1:1 v/v) for 20 min at −20 °C. After washing three times with PBS, unspecific binding was prevented by incubating with 3% BSA in PBS for 30 min at RT. Slices were kept overnight at 4 °C with the primary antibody mouse monoclonal anti-FITC (1:50; Sigma) in PBS containing 0.5% BSA solution. In the next day, brain slices were washed with PBS and then incubated for 1 h, at RT, with the corresponding secondary antibody Alexa Fluor 594 donkey antimouse (1:200; Invitrogen). For nuclear labeling, cell preparations were stained with Hoechst 33342 (2 μg/mL; Invitrogen) in PBS for 5 min, at RT, and mounted in Dako fluorescent medium (Dakocytomation Inc., Carpinteria, CA, U.S.A.). Fluorescent images were acquired using a confocal microscope (LSM 510 Meta, Carl Zeiss).

Statistical Analysis. All experimental conditions were performed in triplicate from 3 independent cell cultures, unless stated otherwise. For SCCI experiments and NeuN immunocytochemistry, measurements were performed in the pseudomonolayer of cells surrounding the seeded SVZ neurospheres. The percentage of neuronal-like responding cells (Hist/KCl ratio <0.8) was calculated on the basis of one microscopic field *per* coverslip, containing approximately 100 cells (40× magnification).

For cell pair assay, 60 cell pairs *per* condition were counted, in triplicate, from five independent cultures. Number of neurospheres in self-renewal assays were measured counting the total number of neurospheres *per* well (from a 24-well plate) in quadruplicate of five independent cultures. Quantification of the number of neuritic ramifications, as well as the total neuritic length positive for P-JNK, *per* neurosphere, was performed in three culture preparations, in approximately 20 nonoverlapping fields *per* coverslip (in triplicate, 20× magnification). The analysis software used was ImageJ (NIH Image, Bethesda, MD, U.S.A.). For qChIP and qRT-PCR *in vitro* experiments, samples were pooled from a 6-well plate, *per* experimental condition. For *in vivo* experiments, a minimum of two animals were used *per* experimental condition in each set of experiments. At least three sets of experiments were performed (minimum of six animals *per* condition).

All experiments included untreated controls or treatment with blank nanoparticles (RA^--NPs) whenever RA^+-NPs were used. Data are expressed as mean ± standard error of mean (SEM). Statistical significance was determined with GraphPad Prism 5 (Graph pad, San Diego, CA, U.S.A.) by using ANOVA followed by Dunnett's or Bonferroni's test or unpaired two-tailed Student's *t* test, with $p < 0.05$ considered to represent statistical significant.

Conflict of Interest: The authors declare no competing financial interest.

Acknowledgment. We thank Cytoviva, Inc. and Dr. Byron Cheatham for performing the hyperspectral imaging analysis. This work was funded by FCT Portugal and by FEDER, PTDC/SAU-NEU/104415/2008 (L.B.), PTDC/SAU-NEU/101783/2008 (F.A.), Grant No. 96542 from the Calouste Gulbenkian Foundation (L.B.; F.A.), and L'Oréal-UNESCO Portugal for Women in Science (L.B.), MIT-Portugal (L.F.), and PTDC/CTM/099659/2008 (L.F.).

Supporting Information Available: Supplementary figures. This material is available free of charge *via* the Internet at http://pubs.acs.org.

REFERENCES AND NOTES

1. Doetsch, F.; Caille, I.; Lim, D. A.; García-Verdugo, J. M.; Alvarez-Buylla, A. Subventricular Zone Astrocytes Are Neural Stem Cells in the Adult Mammalian Brain. *Cell* **1999**, *97*, 703–716.
2. Ming, G.-l.; Song, H. Adult Neurogenesis in the Mammalian Brain: Significant Answers and Significant Questions. *Neuron* **2011**, *70*, 687–702.
3. Sanai, N.; Nguyen, T.; Ihrie, R. A.; Mirzadeh, Z.; Tsai, H.-H.; Wong, M.; Gupta, N.; Berger, M. S.; Huang, E.; Garcia-Verdugo, J.-M.; et al. Corridors of Migrating Neurons in the Human Brain and Their Decline During Infancy. *Nature* **2011**, *478*, 382–386.
4. Santos, T.; Maia, J.; Agasse, F.; Xapelli, S.; Ferreira, L.; Bernardino, L. Nanomedicine Boosts Neurogenesis: New Strategies for Brain Repair. *Integr. Biol.* **2012**, *4*, 973–981.
5. Kubek, M.; Domb, A.; Veronesi, M. Attenuation of Kindled Seizures by Intranasal Delivery of Neuropeptide-Loaded Nanoparticles. *Neurotherapeutics* **2009**, *6*, 359–371.
6. Gao, X.; Tao, W.; Lu, W.; Zhang, Q.; Zhang, Y.; Jiang, X.; Fu, S. Lectin-Conjugated PEG-PLA Nanoparticles: Preparation and Brain Delivery After Intranasal Administration. *Biomaterials* **2006**, *27*, 3482–3490.
7. Maden, M. Retinoic Acid in the Development, Regeneration and Maintenance of the Nervous System. *Nat. Rev. Neurosci.* **2007**, *8*, 755–765.
8. Kastner, P.; Mark, M.; Ghyselinck, N.; Krezel, W.; Dupe, V.; Grondona, J. M.; Chambon, P. Genetic Evidence that the Retinoid Signal is Transduced by Heterodimeric RXR/RAR Functional Units During Mouse Development. *Development* **1997**, *124*, 313–326.
9. Krezel, W.; Kastner, P.; Chambon, P. Differential Expression of Retinoid Receptors in the Adult Mouse Central Nervous System. *Neuroscience* **1999**, *89*, 1291–1300.
10. Bastien, J.; Rochette-Egly, C. Nuclear Retinoid Receptors and the Transcription of Retinoid-Target Genes. *Gene* **2004**, *328*, 1–16.
11. Kim, M.; Habiba, A.; Doherty, J. M.; Mills, J. C.; Mercer, R. W.; Huettner, J. E. Regulation of Mouse Embryonic Stem Cell Neural Differentiation by Retinoic Acid. *Dev. Biol.* **2009**, *328*, 456–471.
12. Stavridis, M. P.; Collins, B. J.; Storey, K. G., Retinoic Acid Orchestrates Fibroblast Growth Factor Signalling to Drive Embryonic Stem Cell Differentiation. *Development 137*, 881-890.

13. Lu, J.; Tan, L.; Li, P.; Gao, H.; Fang, B.; Ye, S.; Geng, Z.; Zheng, P.; Song, H. All-Trans Retinoic Acid Promotes Neural Lineage Entry by Pluripotent Embryonic Stem Cells *via* Multiple Pathways. *BMC Cell Biol.* **2009**, *10*, 57.
14. Wang, T. W.; Zhang, H.; Parent, J. M. Retinoic Acid Regulates Postnatal Neurogenesis in the Murine Subventricular Zone-Olfactory Bulb Pathway. *Development* **2005**, *132*, 2721–2732.
15. Takahashi, J.; Palmer, T. D.; Gage, F. H. Retinoic Acid and Neurotrophins Collaborate to Regulate Neurogenesis in Adult-Derived Neural Stem Cell Cultures. *J. Neurobiol.* **1999**, *38*, 65–81.
16. Corcoran, J.; Maden, M. Nerve Growth Factor Acts *via* Retinoic Acid Synthesis to Stimulate Neurite Outgrowth. *Nat. Neurosci.* **1999**, *2*, 307–308.
17. Hádinger, N.; Varga, B. V.; Berzsenyi, S.; Környei, Z.; Madarász, E.; Herberth, B. Astroglia Genesis *In Vitro*: Distinct Effects of Retinoic Acid in Different Phases of Neural Stem Cell Differentiaion. *Int. J. Dev. Neurosci.* **2009**, *27*, 365–375.
18. Wu, M.; Zhang, Y.; Wu, N. H.; Shen, Y. F. Histone Marks and Chromatin Remodelers on the Regulation of Neurogenin1 Gene in RA Induced Neuronal Differentiation of P19 Cells. *J. Cell. Biochem.* **2009**, *107*, 264–271.
19. Szuts, E. Z.; Harosi, F. I. Solubility of Retinoids in Water. *Arch. Biochem. Biophys.* **1991**, *287*, 297–304.
20. Maia, J.; Santos, T.; Aday, S.; Agasse, F.; Cortes, L.; Malva, J. O.; Bernardino, L.; Ferreira, L. Controlling the Neuronal Differentiation of Stem Cells by the Intracellular Delivery of Retinoic Acid-Loaded Nanoparticles. *ACS Nano* **2011**, *5*, 97–106.
21. Germain, P.; Gaudon, C.; Pogenberg, V.; Sanglier, S.; Van Dorsselaer, A.; Royer, C. A.; Lazar, M. A.; Bourguet, W.; Gronemeyer, H. Differential Action on Coregulator Interaction Defines Inverse Retinoid Agonists and Neutral Antagonists. *Chem. Biol.* **2009**, *16*, 479–489.
22. Agasse, F.; Bernardino, L.; Silva, B.; Ferreira, R.; Grade, S.; Malva, J. O. Response to Histamine Allows the Functional Identification of Neuronal Progenitors, Neurons, Astrocytes, and Immature Cells in Subventricular Zone Cell Cultures. *Rejuvenation Res.* **2008**, *11*, 187–200.
23. Bernardino, L.; Agasse, F.; Silva, B.; Ferreira, R.; Grade, S.; Malva, J. O. Tumor Necrosis Factor-α Modulates Survival, Proliferation, and Neuronal Differentiation in Neonatal Subventricular Zone Cell Cultures. *Stem Cells* **2008**, *26*, 2361–2371.
24. Agasse, F.; Bernardino, L.; Kristiansen, H.; Christiansen, S. H.; Ferreira, R.; Silva, B.; Grade, S.; Woldbye, D. P. D.; Malva, J. O. Neuropeptide Y Promotes Neurogenesis in Murine Subventricular Zone. *Stem Cells* **2008**, *26*, 1636–1645.
25. Schroeder, T. Imaging Stem-Cell-Driven Regeneration in Mammals. *Nature* **2008**, *453*, 345–351.
26. Episkopou, V. Sox2 Functions in Adult Neural Stem Cells. *Trends Neurosci.* **2005**, *28*, 219–221.
27. Doetsch, F.; Petreanu, L.; Caille, I.; García-Verdugo, J.-M.; Alvarez-Buylla, A. EGF Converts Transit-Amplifying Neurogenic Precursors in the Adult Brain into Multipotent Stem Cells. *Neuron* **2002**, *36*, 1021–1034.
28. Shen, Q.; Zhong, W.; Jan, Y. N.; Temple, S. Asymmetric Numb Distribution is Critical for Asymmetric Cell Division of Mouse Cerebral Cortical Stem Cells and Neuroblasts. *Development* **2002**, *129*, 4843–4853.
29. Oliva, A. A., Jr; Atkins, C. M.; Copenagle, L.; Banker, G. A. Activated c-Jun N-Terminal Kinase Is Required for Axon Formation. *J. Neurosci.* **2006**, *26*, 9462–9470.
30. Dilworth, F. J.; Chambon, P. Nuclear Receptors Coordinate the Activities of Chromatin Remodeling Complexes and Coactivators to Facilitate Initiation of Transcription. *Oncogene* **2001**, *20*, 3047–3054.
31. Heintzman, N. D.; Stuart, R. K.; Hon, G.; Fu, Y.; Ching, C. W.; Hawkins, R. D.; Barrera, L. O.; Van Calcar, S.; Qu, C.; Ching, K. A.; et al. Distinct and Predictive Chromatin Signatures of Transcriptional Promoters and Enhancers in the Human Genome. *Nat. Genet.* **2007**, *39*, 311–318.
32. Santos-Rosa, H.; Schneider, R.; Bannister, A. J.; Sherriff, J.; Bernstein, B. E.; Emre, N. C. T.; Schreiber, S. L.; Mellor, J.; Kouzarides, T. Active Genes Are Tri-Methylated at K4 of Histone H3. *Nature* **2002**, *419*, 407–411.
33. Lim, D. A.; Huang, Y. C.; Swigut, T.; Mirick, A. L.; Garcia-Verdugo, J. M.; Wysocka, J.; Ernst, P.; Alvarez-Buylla, A. Chromatin Remodelling Factor Mll1 Is Essential For Neurogenesis From Postnatal Neural Stem Cells. *Nature* **2009**, *458*, 529–533.
34. Ross, S. E.; Greenberg, M. E.; Stiles, C. D. Basic Helix-Loop-Helix Factors in Cortical Development. *Neuron* **2003**, *39*, 13–25.
35. Suslov, O. N.; Kukekov, V. G.; Ignatova, T. N.; Steindler, D. A. Neural Stem Cell Heterogeneity Demonstrated by Molecular Phenotyping of Clonal Neurospheres. *Proc. Natl. Acad. Sci. U.S.A.* **2002**, *99*, 14506–14511.
36. Kim, E. J.; Leung, C. T.; Reed, R. R.; Johnson, J. E. *In Vivo* Analysis of Ascl1 Defined Progenitors Reveals Distinct Developmental Dynamics During Adult Neurogenesis and Gliogenesis. *J. Neurosci.* **2007**, *27*, 12764–12774.
37. Kim, E. J.; Ables, J. L.; Dickel, L. K.; Eisch, A. J.; Johnson, J. E. Ascl1 (Mash1) Defines Cells With Long-Term Neurogenic Potential in Subgranular and Subventricular Zones in Adult Mouse Brain. *PLoS One* **2011**, *6*, e18472.
38. Pastrana, E.; Cheng, L. C.; Doetsch, F. Simultaneous Prospective Purification of Adult Subventricular Zone Neural Stem Cells and Their Progeny. *Proc. Natl. Acad. Sci. U.S.A.* **2009**, *106*, 6387–6392.
39. Lundell, T. G.; Zhou, Q.; Doughty, M. L. Neurogenin1 Expression in Cell Lineages of the Cerebellar Cortex in Embryonic and Postnatal Mice. *Dev. Dyn.* **2009**, *238*, 3310–3325.
40. Liao, W. L.; Tsai, H. C.; Wang, H. F.; Chang, J.; Lu, K. M.; Wu, H. L.; Lee, Y. C.; Tsai, T. F.; Takahashi, H.; Wagner, M.; et al. Modular Patterning of Structure and Function of the Striatum by Retinoid Receptor Signaling. *Proc. Natl. Acad. Sci. U.S.A.* **2008**, *105*, 6765–6770.
41. Kim, E. J.; Hori, K.; Wyckoff, A.; Dickel, L. K.; Koundakjian, E. J.; Goodrich, L. V.; Johnson, J. E. Spatiotemporal Fate Map of Neurogenin1 (Neurog1) Lineages in the Mouse Central Nervous System. *J. Comp. Neurol.* **2011**, *519*, 1355–1370.
42. Voronova, A.; Fischer, A.; Ryan, T.; Al Madhoun, A.; Skerjanc, I. S. Ascl1/Mash1 Is a Novel Target of Gli2 during Gli2-Induced Neurogenesis in P19 EC Cells. *PLoS One* **2011**, *6*, e19174.
43. Oishi, K.; Watatani, K.; Itoh, Y.; Okano, H.; Guillemot, F.; Nakajima, K.; Gotoh, Y. Selective Induction of Neocortical GABAergic Neurons by the PDK1-Akt Pathway Through Activation of Mash1. *Proc. Natl. Acad. Sci. U.S.A.* **2009**, *106*, 13064–13069.
44. Vierbuchen, T.; Ostermeier, A.; Pang, Z. P.; Kokubu, Y.; Sudhof, T. C.; Wernig, M. Direct Conversion of Fibroblasts to Functional Neurons by Defined Factors. *Nature* **2010**, *463*, 1035–1041.
45. Doetsch, F.; Garcia-Verdugo, J. M.; Alvarez-Buylla, A. Regeneration of a Germinal Layer in the Adult Mammalian Brain. *Proc. Natl. Acad. Sci. U.S.A.* **1999**, *96*, 11619–11624.
46. Liu, X. S.; Zhang, Z. G.; Zhang, R. L.; Gregg, S. R.; Meng, H.; Chopp, M. Comparison of *In Vivo* and *In Vitro* gene Expression Profiles in Subventricular Zone Neural Progenitor Cells From the Adult Mouse After Middle Cerebral Artery Occlusion. *Neuroscience* **2007**, *146*, 1053–1061.
47. Johanson, C. E.; Stopa, E. G.; McMillan, P. N. The Blood-Cerebrospinal Fluid Barrier: Structure and Functional Significance. *Methods Mol. Biol.* **2011**, *686*, 101–131.
48. Bharali, D. J.; Klejbor, I.; Stachowiak, E. K.; Dutta, P.; Roy, I.; Kaur, N.; Bergey, E. J.; Prasad, P. N.; Stachowiak, M. K. Organically Modified Silica Nanoparticles: a Nonviral Vector for *In Vivo* Gene Delivery and Expression in the Brain. *Proc. Natl. Acad. Sci. U.S.A.* **2005**, *102*, 11539–11544.
49. Jarvis, C. I.; Goncalves, M. B.; Clarke, E.; Dogruel, M.; Kalindjian, S. B.; Thomas, S. A.; Maden, M.; Corcoran, J. P. T. Retinoic Acid Receptor-α Signalling Antagonizes Both Intracellular and Extracellular Amyloid-β Production and Prevents Neuronal Cell Death Caused by Amyloid-β. *Eur. J. Neurosci.* **2010**, *32*, 1246–1255.
50. Bonnet, E.; Touyarot, K.; Alfos, S.; Pallet, V. r.; Higueret, P.; Abrous, D. N. Retinoic Acid Restores Adult Hippocampal

Neurogenesis and Reverses Spatial Memory Deficit in Vitamin A Deprived Rats. *PLoS One* **2008**, *3*, e3487.
51. Plane, J. M.; Whitney, J. T.; Schallert, T.; Parent, J. M. Retinoic Acid and Environmental Enrichment Alter Subventricular Zone and Striatal Neurogenesis After Stroke. *Exp. Neurol.* **2008**, 125–134.
52. Pfaffl, M. W. A New Mathematical Model for Relative Quantification in Real-Time RT-PCR. *Nucleic Acids Res.* **2001**, *29*, e45.